Open access • Journal Article • DOI:10.1002/MAME.201000174

Lifetime Assessment of Load-Bearing Polymer Glasses: The Influence of Physical Ageing — Source link

H.A. Visser, T.C. Bor, Mannes Wolters, Jgf Joris Wismans ...+1 more authors

Institutions: University of Twente, Eindhoven University of Technology

Published on: 10 Dec 2010 - Macromolecular Materials and Engineering (Wiley-VCH Verlag)

Topics: Fatigue limit, Paris' law and Failure mode and effects analysis

DOI:
Article Type: Full paper

Lifetime assessment of load-bearing polymer glasses; The influence of physical ageing

H.A. Visser*, T.C. Bor, M. Wolters, J.G.F. Wismans, L.E. Govaert

H.A. (Roy) Visser, Ton C. Bor, Mannes Wolters
Faculty of Engineering Technology, University of Twente, P.O.Box 217, NL-7500 AE Enschede, the Netherlands
E-mail: h.a.visser@ctw.utwente.nl

Joris G.F. Wismans, Leon E. Govaert
Materials Technology (MaTe), Eindhoven University of Technology, P.O.Box 513, NL-5600 MB Eindhoven, the Netherlands

Abstract

The timescale at which ductile failure occurs in loaded glassy polymers can be successfully predicted using the engineering approach presented in a previous publication. In this paper the influence of progressive physical ageing on the plastic deformation behaviour of unplasticised poly(vinyl chloride) (uPVC) is characterised and incorporated in the existing approach. With the modification it is possible to quantitatively predict long-term failures which show a so-called endurance limit. The predictions are compared with failure data of uPVC specimens which were subjected to constant or dynamic loads. In dynamic loading conditions a second type of failure mode was observed: fatigue crack growth. A brief study on the influence of the frequency and stress ratio of the applied stress signal shows that crack growth failure is not expected to occur within experimentally reasonable timescales for constant loading conditions.

Introduction

Since the 1950's polymer pipes have been installed in water and gas distribution systems throughout the world. The same holds for the Dutch gas distribution network,

in which a significant number of polymer pipes has been installed in the first decade after the discovery of the Slochteren gas field in 1959. The service life of these pipes was initially specified to be 50 years. This means that replacement based on the time a pipe has been in service will lead to the renewal of thousands of kilometres of pipelines in the near future. Since replacement of these distribution systems is labour intensive, its postponement will result in huge economic savings for society. On the other hand, the integrity of the network should not be compromised, especially in the case of gas distribution networks where failure can lead to life threatening situations.[1,2] Consequently, the prediction of the residual lifetime of polymer pipes has received considerable attention, (see for example[3–6]). As the lifetimes of the pipes can exceed 50 years, accelerated tests have been developed to determine the lifetime based on short-term tests. The most well known tests used for this purpose are experiments where the failure time of a pipe segment that is subjected to a constant internal pressure is measured. The lifetime is estimated by extrapolating the time-to-failure measured at testing conditions (mostly at elevated temperatures) towards a reference condition according to a method described in ISO 9080. A typical result is shown schematically in Figure 1 (left). In general three regions can be observed with each having different failure mechanisms.[3,7,8] In the high stress region (region I) the pipe segment shows a considerable amount of plastic deformation before failure. The pipe bulges until the tensile strength is reached locally and rupture occurs. A model for the deformation kinetics can be employed to make quantitative predictions of the failure time of these ductile failures, as has been shown in a previous paper.[9] At lower stresses a knee can be observed in the curve describing the failure kinetics, which is sometimes referred to as the "mechanical knee".[8] The failure in region II is attributed to slow crack growth, leading to a hairline crack. The hairline crack is a slit in axial direction with a small plastic zone at the ends. Various models exist that can predict the failure kinetics in regime II quantitatively, most of which are based on a fracture mechanics approach to calculate the crack growth rate (e.g.[5,10,11]). Failure in the third region is related to progressive molecular degradation leading to the formation of multiple cracks.[7,12] The subsequent time-to-failure is almost independent of the applied stress.

In this study the focus will be on the long-term behaviour of unplasticised poly(vinyl chloride) (uPVC) pipes, which have been used extensively in the gas, water and sewer distribution networks in the Netherlands. Increased knowledge on the stabilisation of uPVC[13,14] and the influence of processing conditions on the mechanical properties , [15,16] has led to prolonged region III and region II failure times. As a result, the long-term behaviour of the pipes is improved considerably and region I failure has become the limiting region for a wider range of failure times. The predictive approach for region I failure as presented in a previous paper[9] is based on the hypothesis that the polymer fails when the accumulated plastic strain reaches a critical value and the polymer enters its softening regime. This approach proved successful to quantitatively

predict long-term failure of pipes subjected to a constant internal pressure as shown in Figure 2 (left). Remarkably, the predictions not only hold for the ductile failures, but also for pipes which failed as a result of hairline cracks. This is in line with the statement of Niklas et al.[17] that slow crack growth did not significantly contribute to the failure time of the PVC pipes they subjected to an internal pressure. Based upon the experimental observation that all failure modes showed similar circumferential strain behaviour up to failure, they stated that all failure modes followed a common path up to failure. Where Niklas et al. modelled the complete visco-elastic creep behaviour to predict failure for pressurised pipes, it was demonstrated that capturing the secondary creep alone is sufficient for quantitative failure predictions.[9]

Here, the hypothesis is posed that the transition from ductile failure towards hairline cracking is caused by time-dependent changes in the mechanical properties of uPVC as a result of physical ageing. This phenomenon finds its origin in the fact that glassy polymers like uPVC[a] are not in a state of thermodynamic equilibrium, but display a continuous strive towards it.[18] As a consequence, the volume decreases, whereas the yield stress increases gradually over time.[19] The increase of the yield stress leads to increased strain softening, which has a strong influence on the failure mode of this type of materials. In general, increased strain softening leads to a stronger strain localisation.[20–23] Eventually, the plastic zone localises to such an extent that cavitation takes place and a craze is initiated.[24] When the craze breaks down, a crack is formed which acts as an extremely sharp notch. The subsequent crack growth occurs at such a high rate that the time it takes for the crack to grow to a critical level does not significantly contribute to the overall failure time.[25] This explains why a different failure mode is observed macroscopically, whereas the path up to failure (accumulation of plastic strain up to a critical value) is, in essence, the same.

Klompen et al.[26] observed a similar transition from ductile to a brittle failure mode for polycarbonate tensile bars subjected to a static load. They showed that the transition can indeed be attributed to an increase in yield stress resulting from progressive physical ageing, i.e. ageing occurring during the experiment itself, confirming the posed hypothesis. They also showed that the increase in yield stress not only influences the failure mode, but the progressive increase in resistance against plastic deformation also leads to the occurrence of a so-called endurance limit. Such a limit under which no failure is observed within experimentally acceptable timescales has been observed for several glassy polymers under deadweight load.[27–30] Despite the change in failure mode, such a change in kinetics is not apparent in the experimental data of Niklas et al.[17] Comparable measurements by Benjamin,[15] as reproduced in Figure 2 (right), do show an endurance limit. The solid lines represent predictions of the current approach that do not take physical ageing into account. The predictions clearly underestimate

[a] Although PVC can have a crystallinity of up to 10% its mechanical properties closely relate to those found for other amorphous (glassy) polymers.

the failure time observed experimentally, especially at 60 °C.

In the present study the physical ageing kinetics is incorporated in the existing engineering approach as presented in a previous paper.[9] The procedure employed in this work is similar to the procedure Klompen et al.[31] used to incorporate the kinetics of physical ageing into their constitutive model. In the resulting engineering approach the time-to-failure follows from a closed form expression. Moreover, it is shown that the more laborious characterisation and numerical calculations of the constitutive approach of Klompen et al. can be circumvented for simple structures subjected to 3D loads. In the next section this procedure for implementing the ageing kinetics is described and the relevant expressions are elucidated. Subsequently, the physical ageing kinetics including its dependence on temperature and stress, is characterised using short-term tensile experiments. To conclude, the approach is validated on experimentally obtained failure data for tensile specimens subjected to either constant or dynamic loads.

Theoretical background

The existing approach[9] is based on the hypothesis that ductile failure occurs when the accumulated plastic strain reaches a critical value, where the polymer enters its softening regime. A pressure-modified Eyring relation[32] was employed to calculate the equivalent plastic strain rate ($\dot{\bar{\gamma}}$) for a given temperature (T), pressure (p) and equivalent stress ($\bar{\tau}$):

$$\dot{\bar{\gamma}}(T, p, \bar{\tau}) = \dot{\gamma}_0 \cdot \exp\left(\frac{-\Delta U}{RT}\right) \cdot \sinh\left(\frac{\bar{\tau}\nu^*}{RT}\right) \cdot \exp\left(\frac{-\mu p \nu^*}{RT}\right), \tag{1}$$

with R to denote the universal gas constant. The pre-exponential factor ($\dot{\gamma}_0$) in Equation (1) is related to the entropy of the system and thus the thermodynamic state of the polymer. The more the polymer has aged, the lower the value of $\dot{\gamma}_0$ will be, reflecting the increased resistance against plastic deformation of the aged glassy polymer. The first exponential term includes the influence of temperature on the plastic strain rate using activation energy (ΔU). In the second term the activation volume ν^* determines the sensitivity of the plastic strain rate to the stress. The third term is included to take the influence of the hydrostatic pressure p into account via the pressure dependence parameter μ, making Equation (1) valid for any 3D loading geometry. Each of the parameters was determined using short-term tensile tests on the uPVC pipe material.[9] The definitions of the equivalent plastic strain rate ($\dot{\bar{\gamma}}$), the equivalent stress ($\bar{\tau}$) and the hydrostatic pressure (p) are given in Table 1.

Brady et al.[20] and Matz et al.[33] showed that the stress and temperature dependence (and hence the activation volume and energy) of polycarbonate are influenced by

an annealing treatment. In other studies[34,35] is was showed, however, that the deformation kinetics can still be described accurately using constant values for the activation volume and energy. Klompen et al.[31] proposed to make only $\dot{\gamma}_0$ in Equation (1) a function of time (t) to incorporate the influence of physical ageing. Here, a similar function is used to describe the behaviour of uPVC:

$$\dot{\gamma}_0(T, \bar{\tau}, t) = b_0 \cdot \left(\frac{t_{eff}\,(T, \bar{\tau}, t) + t_a}{t_0} \right)^{b_1}, \tag{2}$$

where b_0 and b_1 are constants[b] and t_0=1 s. The initial age of the specimen is denoted as t_a, which is related to the thermo-mechanical history of the material. As it is well known that the process of physical ageing is accelerated by temperature[19] and stress and strain,[31,36–40] the effective time (t_{eff}) is introduced. The effective time is a measure for the ageing time t at reference conditions (zero stress and T=T_{ref}) and is related to the ageing time at temperature T and stress $\bar{\tau}$ via the acceleration factors a_T and a_σ, respectively. The effective time is defined as:

$$t_{eff} = \int_0^t \frac{\mathrm{d}t'}{a_T(T) \cdot a_\sigma(T, \bar{\tau})}, \tag{3}$$

where a_T is the temperature-induced acceleration factor and a_σ the stress-induced acceleration factor. These acceleration factors are equal to unity for the reference condition. The relation for the plastic deformation rate including the influence of physical ageing can now be obtained by combining Equation (1), (2) and (3):

$$\dot{\bar{\gamma}}(T, p, \bar{\tau}, t) = \frac{b_0}{t_0^{b_1}} \cdot \left(\int_0^t \frac{\mathrm{d}t'}{a_T(T) \cdot a_\sigma(T, \bar{\tau})} + t_a \right)^{b_1} \cdots \\ \cdot \exp\left(\frac{-\Delta U - \mu p \nu^*}{RT} \right) \cdot \sinh\left(\frac{\bar{\tau}\nu^*}{RT} \right). \tag{4}$$

As failure occurs when the accumulated plastic strain reaches a critical level, the time-to-failure can be found by integrating the rate of plastic deformation (Equation (4)) up to the critical equivalent strain.

$$\bar{\gamma}_{acc} = \int_0^t \dot{\bar{\gamma}}(T, p, \bar{\tau}, t)\,\mathrm{d}t, \qquad \text{failure occurs if:} \quad \bar{\gamma}_{acc} = \gamma_{cr} \tag{5}$$

This relation can be used to deduct analytical expressions for the time-to-failure for different load cases. In the validation procedure, which follows after the

[b]The constants b_0 and b_1 presented here are directly related to some of the ageing parameters in the work of Klompen et al.[31]: b_0=$\dot{\gamma}_{0,rej} \cdot \exp(-c_0)$ and b_1=$\frac{-c_1}{\ln(10)}$.

characterisation of the physical ageing kinetics of uPVC, the expressions for a constant and a dynamic (triangular) tensile load are given.

Experimental

Material and specimen preparation

The uPVC specimens were taken out of an excavated uPVC gas distribution pipe that was in service for several decades. The pipe has a diameter of 160 mm and a wall thickness of about 4.1 mm. A section of 70 mm was cut from the pipe with a bandsaw and subsequently sawed in half in axial direction. These parts were then pressed into flat plates in a press at 100 °C,[c] thus approximately 20 °C above the glass transition temperature of uPVC, in 25 minutes at a pressure of approximately 1 MPa. This procedure erased all prior effects of physical ageing, thus $\dot{\gamma}_0$ of the specimens that are manufactured in this way is only dependent on the cooling rate in the cold press and subsequent heat treatments. Tensile bars with a gauge section of approximately $30\times5\times4.1$ mm^3 were milled from the plate material with the length direction of the tensile bars parallel to the axial direction of the pipe. The specimens which were used to characterise the ageing kinetics were given an annealing treatment in an convection oven (at a temperature of 45 °C, 55 °C or 65 °C) or by storing them at ambient conditions (25 °C).

The compact tension specimens were milled from plates that were produced in the same way as the ones used for producing the tensile specimens. The geometry of the compact tension specimens is in accordance with the ASTM E-647 standard, and have a characteristic width of 32 mm (from backside to center of holes). The notch was machined in the axial direction of the original pipe.

Experimental setup

All uniaxial tensile, creep and fatigue crack growth measurements were carried out on an MTS Elastomer Testing System 810 equipped with a 25 kN force cell or a Zwick Z010 equipped with a 2.5 kN force cell. Engineering stresses were calculated using the average of the cross-sectional surface areas as measured at three locations in the gauge section of the specimen. The tensile experiments were carried out at a constant crosshead speed, thus at a constant *engineering* strain rate. The creep tests

[c] It is known that a heat treatment at 100 °C can influence the crystallinity of the uPVC.[41] A change in crystallinity can have marked effect on the physical ageing behaviour of uPVC.[42] As all specimens used throughout this study received the same preparation procedure, differences in ageing behaviour are not to be expected.

were conducted at a constant load, thus at constant *engineering* stress. For all fatigue tests a triangular signal was used. Two sets of fatigue tests were conducted. For the first set of experiments the minimum stress was kept at a constant level of 2.5 MPa while varying the maximum stress level and frequency of the stress signal. The second set of fatigue experiments was conducted at three different levels of the stress ratio (minimum stress/maximum stress level) for a range of maximum stresses and a frequency of 1 Hz.

The fatigue crack growth measurements were carried out with a sinusoidal stress signal with a frequency of 1 Hz and at four different stress ratios. The crack growth was monitored with the use of a video camera.

Ageing kinetics of uPVC

At room temperature uPVC is about 60 °C below its glass transition temperature, T_g, and about 60 °C above its β-transition. Although the main chain segmental mobility is low at room temperature, it is sufficient to allow for small conformational changes towards their thermodynamically favoured positions.[18] With annealing, defined here as a heat treatment at a temperature below T_g, this process can be accelerated, which makes the ageing effect more apparent at shorter timescales.

The influence of annealing at four different temperatures on the yield stress of uPVC tensile specimens as measured at 25 °C and a strain rate of 10^{-3} s^{-1} is shown in Figure 3. The yield stress increases about 20% after an annealing treatment of $2.3 \cdot 10^6$ s (corresponding to almost a month) at 65 °C. The data for the different annealing temperatures can be shifted towards one single curve, using only horizontal shift factors. The natural logarithm of the horizontal shift factors are plotted versus the inverse of the annealing temperatures in Figure 4. The data can be accurately described with a linear relation. This suggests that an Arrhenius type of time-temperature superposition can be employed to calculate the shift factor a_T:

$$a_T(T_a) = \exp\left(\frac{\Delta U_a}{R} \cdot \left(\frac{1}{T_a} - \frac{1}{T_{ref}}\right)\right) , \tag{6}$$

where the activation energy (ΔU_a) can be calculated from the slope of the best fit in Figure 4, resulting in a value of 115 kJ $\cdot$ mol^{-1}. The temperature during annealing is denoted as T_a and T_{ref} is the reference temperature. A clear distinction should be made between T_a and T_{ref} in Equation (6) and the temperature T in Equation (1) at which the tensile test is carried out. T_a influences the ageing kinetics, T_{ref} the timescale of the mastercurve and T the plastic deformation rate. The mastercurve resulting from shifting the yield data in Figure 3 to a reference temperature of 25 °C with Equation (6) is shown in Figure 5. This mastercurve can be described with Equation (4), for which the initial age of the specimens (t_a) and the constants b_0 and b_1 were obtained using

a non-linear least squares fitting routine. The value for the initial age determines the length of the time-independent initial plateau and depends on the thermo-mechanical history of the material. The values of b_0 and b_1 determine the position and slope of the time-dependent yield behaviour. The value for b_0 depends on the choice of the reference temperature and b_1 is only material dependent. With the non-linear least squares fitting routine a best fit was found with b_0=1.13 $\cdot 10^{44}$ s^{-1} (at T_{ref}=25 °C), b_1=0.95 and t_a=4.9 $\cdot 10^5$ s. The latter value implies that ageing will occur already after one week at T_a=T_{ref} and $\bar{\tau}_a$=0 MPa. The fit is shown as a solid line in Figure 5 and accurately follows the experimental results.

As already stated, the segmental mobility of polymer chains in a glassy polymer is also known to increase by applying a mechanical load, resulting in mechanically enhanced ageing[31,36–40] (also referred to as stress/strain induced ageing). The kinetics of stress-induced ageing are characterised by first subjecting specimens to a constant tensile stress of 25 MPa or 32.5 MPa for a range of ageing times. Subsequently, the cross-sectional area of the specimens is measured again and a tensile test is performed at a strain rate of 10^{-3} s^{-1} at 25 °C.[d] The resulting yield stress data are shown in Figure 6. The mastercurve at T=T_a=25 °C is shown as a solid line in the same figure. This mastercurve can be shifted towards the yield stress data of the aged specimens using an Eyring type time-stress superposition as proposed by Tervoort et al.:[43]

$$a_\sigma(T_a, \bar{\tau}_a) = \frac{\bar{\tau}_a \nu_a}{RT_a} \cdot \sinh\left(\frac{\bar{\tau}_a \nu_a}{RT_a}\right)^{-1}. \tag{7}$$

Constructing a master curve of the experimental data with the use of Equation (7) with ν_a as a fit parameter, resulted in a value of 9.65 $\cdot 10^{-4}$ m$^3 \cdot$ mol^{-1}. With this value of ν_a a good fit of the dashed lines is obtained (see Figure 6).

The parameters that followed from the characterisation of the temperature and stress-induced ageing kinetics of uPVC are summarised in Table 2. The next step is to verify whether the approach can successfully predict the influence of progressive physical ageing during creep and fatigue experiments.

Validation using uniaxial tensile creep failure data

The method is validated first with the use of creep failure data. In a previous paper,[9] it has been shown that the time-to-failure could be predicted employing Equation (1) to

[d]The tensile measurements of the specimens aged at 25 MPa and 32 MPa were carried out at a temperature lower than 25 °C. As the temperature during the tensile test has a marked influence on the yield stress (about 0.75 MPa/K around room temperature), the measured tensile yield stress is compensated to comply with a testing temperature of 25 °C with the use of Equation (1) and the parameters determined previously.[9]

calculate the accumulation of the plastic strain up to a critical equivalent plastic strain ($\bar{\gamma}_{cr}$) for uPVC subjected to a constant tensile load. The predictions proved to agree quantitatively with experimental measurements as long as physical ageing did not have a significant influence. Beyond this point the influence of physical ageing emerges as the resistance against plastic deformation increases, leading to progressively longer failure times. With the use of Equation (4) and (5), this influence of physical ageing is taken into account for failure time predictions.

The deduction of the closed form solution of Equation (5) for isothermal, constant stress conditions (creep tests) can be found in Appendix A. The equivalent stress and the hydrostatic pressure for specimens subjected to uniaxial tension can be calculated using the definitions given in Table 1 and are given in Table 3. During a creep test the ageing temperature is equal to the testing temperature and the ageing stress equal to the applied stress (σ), thus T_a=T and $\bar{\tau}_a$=$\frac{\sigma}{\sqrt{3}}$. For the time-to-failure this results in:

$$t_f(T,\sigma) = a_T(T)\cdot a_\sigma(T,\frac{\sigma}{\sqrt{3}})\cdots \\ \cdot\left(\left[\frac{\bar{\gamma}_{cr}\cdot t_0^{b_1}\cdot(b_1+1)\cdot\exp\left(\frac{\Delta U}{RT}-\frac{\mu\sigma\nu^*}{3RT}\right)}{a_T(T)\cdot a_\sigma(T,\frac{\sigma}{\sqrt{3}})\cdot b_0\cdot\sinh\left(\frac{\sigma\nu^*}{\sqrt{3}RT}\right)}+t_a^{b_1+1}\right]^{\frac{1}{b_1+1}}-t_a\right). \quad (8)$$

The only unknown parameter in this relation is the initial thermodynamic state represented by the initial age (t_a). This parameter can be calculated from the yield stress of a specimen which has the same thermo-mechanical history as the specimens used in the creep tests. The relation between initial age and the yield stress as measured at a certain strain rate ($\dot{\epsilon}$) and temperature is obtained by rewriting Equation (4):

$$t_a = \left(\frac{\sqrt{3}\dot{\epsilon}\cdot t_0^{b_1}\cdot\exp\left(\frac{3\Delta U-\mu\sigma_y\nu^*}{3RT}\right)}{b_0\cdot\sinh\left(\frac{\sigma_y\nu^*}{\sqrt{3}RT}\right)}\right)^{\frac{1}{b_1}}. \quad (9)$$

The experimentally obtained time-to-failure data is shown for two different sets of specimens in Figure 7. The first set is referred to as “annealed” and was annealed for $5\cdot10^5$ s at 60 °C. The other set is referred to as “as manufactured” and did not receive a heat treatment after the production procedure as described in the experimental section. The annealed specimens were tested at a temperature of 20 °C, whereas the as-manufactured specimens were tested at 24 °C. Therefore, the difference between the failure times of the two sets of specimens cannot be attributed solely to the difference in thermal history, but is partly a testing temperature effect (for about 3 MPa).

The initial age as determined using the tensile yield stress of each set of specimens

is found to be $9.1 \cdot 10^7$ s and $1.4 \cdot 10^6$ s for the annealed and as-manufactured specimens respectively (T_{ref}=25 °C). The time-to-failure predictions which follow from Equation (8) are shown as solid lines in Figure 7. The dashed lines in this figure represent failure predictions of the approach excluding the influence of physical ageing. Ageing does not influence the failure kinetics for short failure times. In this regime both predictions are in agreement with the experimental data. At longer failure times the influence of ageing becomes apparent. For the as-manufactured specimens this occurs at failure times longer than about 10^3 s. At these timescales the resistance against plastic deformation of the specimen changes during the creep test, mainly owing to stress-induced ageing. The predicted endurance limit[e] is in quantitative agreement with the one observed experimentally. For the annealed specimens no endurance limit was observed experimentally, which is in agreement with the theoretical prediction that ageing effects appear for failure times longer than about 10^5 s. This marked difference with the as-manufactured specimens is a direct result of the difference in the initial age of the two sets of specimens caused by the ageing procedure of the annealed specimens.

Employing Equation (8) to predict the long-term failure data of PC as presented by Klompen et al.[26] results in a prediction that is comparable to their prediction. It is noteworthy that whereas Klompen et al. used a model incorporating the full constitutive behaviour of PC to calculate the failure times, here the predictions follow from a closed-form analytical relation (Equation (8)).

Validation using failure data for internally pressurised pipes

In a previous publication [9] it was shown that the engineering approach is able to predict the time-to-(ductile)failure of glassy polymers subjected to different loading geometries, such as that found in a pipe subjected to an internal pressure. The extended version of the engineering approach as presented in the present paper is validated by predicting the time-to-failure for two sets of failure data for pressurised pipes from different sources. The first set comprises failure data of pipes under an internal pressure as presented by Niklas et al.[17] that are reproduced in Figure 8. Two types of predictions were calculated. The dashed lines represent the prediction for the approach in which physical ageing effects were not taken into account. The predictions represented as solid lines do include these effects. The initial age is calculated using one reference point and Equation (9), resulting in a value of $2.3 \cdot 10^8$ s which is relatively high when compared to the initial age values found for the tensile

[e] Although no mathematical lower stress limit exists in Equation (8) where t_f becomes infinitive, such a limit is experienced within experimentally realistic timescales. As mentioned earlier, this "limit" is referred to as the endurance limit.

specimens used in this study. This explains why the prediction that neglects the influence of physical ageing, holds so well up to very long failure times. Furthermore, it is noteworthy that the transition from ductile failure to hairline cracking indeed occurs in the region where the solid lines start to deviate from the dashed lines; thus, where the approach predicts a change in yield behaviour as a result of physical ageing. This supports the hypothesis that the transition to hairline cracking is governed by physical ageing, leading to a more localised deformation behaviour. The transition sets in when a certain thermodynamic state is reached, which, in this case, occurs directly when ageing becomes apparent. These two transitions do not necessarily have to be connected as can be seen in the other set of experimental pipe failure data that is predicted next.

The second set of failure data of pipes was presented by Benjamin[44] who studied the influence of the level of gelation on the time-to-failure of pipes. As already stated in the introduction, the increased knowledge on stabilisation and processing has led to improved service lifetimes of uPVC pipes. Especially the processing conditions have a significant influence on the mechanical properties of the uPVC product. The degradation temperature of PVC is lower than the the melting temperature at which the primary particle structure[f] within the PVC grains is destroyed, thus uPVC, unlike most other polymers, cannot be processed from the melt. Destroying the primary particle structure is therefore difficult, and poor processing can result in a PVC product in which the primary particle structure is still partly intact. This primary particle grains can act as stress concentrators in the final product, influencing its mechanical properties. The level of gelation is related to the degree in which the primary PVC particle structure is destroyed during processing and thus a measure for the homogeneity of the molecular structure (e.g.[45,46]). A significant part of the Dutch gas distribution network was installed in the period from the sixties up to the mid-seventies using uPVC pipes, when the developments in processing were still taking place. Evaluation of used pipe segments from this production period showed that the degree of gelation of these pipes varies from poor to "over-gelled" (thermally degraded).[47] The failure data from Benjamin[15] (reproduced in Figure 9) are used to study the influence of the level of gelation on the ageing kinetics. Benjamin subjected four different sets of uPVC pipes to a constant internal pressure at two temperatures. Each set was processed under different extrusion conditions resulting in a range of gelation levels; from very poor gelation (32%), up to so-called over-gelation (90%). It is well known that the level of gelation has a marked influence on mechanical properties like impact strength and strain at break.[15,48–52] The yield properties of uPVC, however, are insensitive for the level of gelation.[15,49–51] This is also demonstrated in Figure 8; the failure kinetics, including the development of an

[f] A comprehensive description of a working model of the particulate structure of PVC is given by Portingell [45]

endurance limit, are equal for all four levels of gelation. The initial age is calculated using one reference point and is only $1.2 \cdot 10^6$ s. This supports the strong influence of physical ageing at relatively short failure times in the experimental data. The predicted influence of the ageing kinetics agrees reasonably well with the measurements at 20 °C, but is somewhat conservative for the measurements at 60 °C. Nonetheless, the approach gives quite an accurate prediction for the level of stress that can be sustained for a certain amount of time.

Like the data of Niklas et al., the data of Benjamin show a transition towards a brittle failure mode. In the data of Benjamin, however, this transition in failure mode is accompanied by a transition in failure kinetics and a knee is observed. Only for the lowest level of gelation region II failure is observed. For low levels of gelation the primary particle structure is still partly present, which can act as a stress concentrator, leading to slow crack growth failure. For increased levels of gelation, the size of the initial flaws caused by the primary particle structure are expected to decrease, shifting region II failure towards longer failure times. Some remarks on region II (crack growth) failure are given at the end of this paper.

Validation using dynamic fatigue data

The predictions for the evolution of yield stress are shown to hold for constant loads. In water distribution networks oscillating pressures caused by opening and closing valves are common.[53] Oscillations in the applied stress are known to accelerate the stress-induced ageing process, when compared to a constant mean stress[54]. Predictions of the proposed engineering approach are compared with data for uPVC tensile bars under a cyclic load in this section, to verify whether the proposed approach can adequately take dynamic stress effects into account.

Modelling dynamic fatigue failure

The triangular stress signal as applied on the tensile bars is shown schematically in Figure 10. By calculating the equivalent plastic strain rate for small timesteps with Equation (1), the accumulation of the plastic strain can be determined. The accumulated plastic strain (excluding the influence of physical ageing) is plotted as a function of time in Figure 11. The figure clearly shows that the plastic strain accumulates differently for a triangular stress signal than during a creep test at the mean stress level (σ_m) of the triangular signal. Therefore, the solution for the time-to-failure as found for constant loads (Equation (8)) cannot be employed directly for a dynamic load. An acceleration factor for the deformation kinetics ($a_{d,\dot{\bar{\gamma}}}$) similar to the one proposed by Janssen et al.,[55] is applied to circumvent a numerical procedure

to find the failure time for dynamic stress signals. The acceleration factor is defined as the accumulated plastic strain after one triangular stress cycle (excluding physical ageing effects), divided by accumulated plastic strain for a constant stress with a value equal to σ_m during the time of one cycle (=1/f):

$$a_{d,\dot{\bar{\gamma}}}(T,\sigma(t')) = \frac{\displaystyle\int_0^{1/f} \left\{ \exp\left(\frac{\mu\,\sigma(t')\nu^*}{3RT}\right) \cdot \sinh\left(\frac{\sigma(t')\nu^*}{\sqrt{3}RT}\right)\right\} \,\mathrm{d}t'}{\dfrac{1}{f}\cdot \exp\left(\dfrac{\mu\sigma_m\nu^*}{3RT}\right) \cdot \sinh\left(\dfrac{\sigma_m\nu^*}{\sqrt{3}RT}\right)}. \tag{10}$$

The solution for a triangular and a square wave of this acceleration factor is deducted in the appendix of Janssen et al.[55] For a triangular waveform the solution is given by:

$$a_{d,\dot{\bar{\gamma}}} = \frac{\sinh\left(\dfrac{\sigma_{amp}}{\sigma_0}\right)}{\dfrac{\sigma_{amp}}{\sigma_0}}, \qquad \text{with:} \quad \sigma_0 = \frac{3RT}{(\mu+\sqrt{3})\cdot\nu^*}. \tag{11}$$

According to this result the acceleration factor for the triangular signal is independent of the frequency of the stress signal, which is consistent with the experimental data of Janssen et al.[55] The equivalent plastic strain rate for a dynamic stress signal can be calculated by multiplying Equation (10) with Equation (1), resulting in the dashed line in Figure 11. The dashed line deviates from the solid line during each cycle, but the accumulated plastic strains are equal after each whole cycle. The error in the predicted failure time is smaller than $(t_f f)^{-1}$ when using the acceleration factor. The accuracy of the predictions thus increases when the cycle time of the stress signal becomes much shorter than the time-to-failure.

Not only the plastic deformation kinetics, but also the ageing kinetics are influenced by a dynamic stress signal. The evolution of the effective time as defined in Equation (3) for a dynamic stress signal can also be calculated using an acceleration factor ($a_{d,age}$), which is defined in a similar way as $a_{d,\dot{\bar{\gamma}}}$:

$$a_{d,age}(T_a,\sigma(t')) = f\cdot a_\sigma\left(T_a,\frac{\sigma_m}{\sqrt{3}}\right)\cdot\int_0^{1/f}\frac{\mathrm{d}t'}{a_\sigma\left(T_a,\frac{\sigma(t')}{\sqrt{3}}\right)}. \tag{12}$$

The deduction of the analytical solution for a triangular wave form is given in Appendix B. This acceleration factor is also found to be independent of the frequency. The effective time for a dynamic stress signal can be calculated by multiplying Equation (3) with Equation (12).

The closed form solution of the time-to-failure for a creep test can be rewritten to give

the time-to-failure for a specimen under isothermal, uniaxial, dynamic tensile stress conditions using the two acceleration factors $a_{d,\dot{\bar{\gamma}}}$ and $a_{d,age}$:

$$t_f(T,\sigma_m,\sigma_{amp}) = \frac{a_T(T)\cdot a_\sigma(T,\frac{\sigma_m}{\sqrt{3}})}{a_{d,age}(T,\sigma_m,\sigma_{amp})}\cdots$$
$$\cdot\left[\left(\frac{a_{d,age}(T,\sigma_m,\sigma_{amp})\cdot\bar{\gamma}_{cr}\cdot t_0^{b_1}\cdot(b_1+1)}{a_T(T)\cdot a_\sigma(T,\frac{\sigma_m}{\sqrt{3}})\cdot a_{d,\dot{\bar{\gamma}}}(T,\sigma_m,\sigma_{amp})\cdot b_0}\cdot\sinh\left(\frac{\sigma_m\nu^*}{\sqrt{3}RT}\right)^{-1}\right.\right.$$
$$\left.\left.\cdot\exp\left(\frac{\Delta U}{RT}-\frac{\mu\sigma_m\nu^*}{3RT}\right)+t_a^{b_1+1}\right)^{\frac{1}{b_1+1}}-t_a\right]. \quad (13)$$

Both $a_{d,\dot{\bar{\gamma}}}$ and $a_{d,age}$ are frequency independent, which makes the time-to-failure also frequency independent.

Frequency dependence

In this section the frequency independent failure behaviour as predicted by the relations presented in the previous sections is verified. Two different sets of uPVC tensile specimens were subjected to a triangular cyclic load at a range of maximum stresses and a constant minimum stress of 2.5 MPa, for various frequencies. One set was annealed for $2.2\cdot10^6$ s at a temperature of 60 °C ("annealed"), the other set of specimens did not receive any additional heat treatment ("as manufactured"). The experimental results for the time-to-failure are shown in Figure 12. The most striking result is that two types of failure kinetics are observed. The failure kinetics in the high stress region (region I, referred to as "yield line" in fatigue studies) is dominated by plastic deformation and has been the failure mode of interest in the present research so far. The region II failure mode observed at lower stresses (grey markers) is presumably related to fatigue crack growth failure, as visual inspection of these specimens points out the existence of crack sites at which the failures initiated.

As anticipated, the yield line is frequency independent, whereas the fatigue crack growth failures shift towards longer failure times with a decrease in frequency. Furthermore, the yield line is clearly influenced by the annealing treatment; the line is shifted almost two decades towards longer failure times. On the other hand, crack growth appears to be uninfluenced by the annealing treatment. More data for multiple sets of specimens at different thermodynamic states are required to confirm this observation. Only the yield line is of interest for validating the presented approach for plastic deformation and ageing kinetics. The region II failures will be discussed in more detail at the end of this paper.

The predictions are again shown as solid and dashed lines for the approach including

and excluding ageing kinetics. The initial age of each set of specimens is calculated from one reference point. The short failure times are predicted accurately, but the experimental data for the as-manufactured specimens level off at somewhat shorter failure times than the theoretical predictions. The ageing trend is captured reasonably well by the engineering approach, but is somewhat conservative. A similar but much more pronounced deviation was reported by Janssen et al.[54] for polycarbonate. This seems to suggest that the material ages somewhat faster for dynamic loading conditions than predicted. The subtle difference between the influence of a constant and dynamic stress signals on the ageing rate is not yet fully understood.

Stress ratio dependence

The experimental failure data presented in the previous section was measured for signals with a changing σ_{max}, but a constant σ_{min} (=2.5 MPa). In this section the influence of a change in stress ratio (R=$\sigma_{min}/\sigma_{max}$) is studied. The difference in stress signal for three levels of R and for a creep test (R=1) is shown in Figure 13. The resulting (predicted) failure times are shown in Figure 14 for these four stress signals. The failure times are shorter for ductile (yield) failures when the stress ratio increases towards unity; the time at high stress levels increases, increasing the rate at which the plastic deformation accumulates. Consequently, the critical level of plastic strain is reached in a shorter timeframe, and the failure time decreases. The failure time for creep tests shifts about 1.4 decade towards longer failure times for specimens subjected to a dynamic stress with a stress ratio of 0.1. The non-linear relation between the stress and the strain rate leads to the effect that the difference in failure time between R=0.1 and R=0.5, is much less pronounced than the difference between R=0.5 and R=1. This behaviour is also observed experimentally: the failure times for the dynamic stresses at the three different stress ratios are within a tight range. Now it has been shown that the proposed engineering approach is capable of predicting the yield failure behaviour (including the influence of the frequency and the stress ratio of the applied stress signal), the behaviour of the other failure mechanism that is observed in the presented failure data is discussed.

Some preliminary remarks on crack growth

A knee was observed in the failure data of the fatigue measurements. The specimens that failed in the region after the knee are filled with surface cracks, which suggests the specimens have failed because of a fatigue crack growth mechanism. This mechanism is comparable to slow crack growth failure of a specimen subjected to a constant load in the sense that in both cases an inherent flaw grows as a result of a load and

eventually causes the specimen to fail. Remarkably, the creep failure data of the tensile bars (Figure 7) and the data of Niklas et al. (Figure 8) did not show any transition towards slow crack growth failure. The question arises as to why this failure mechanism was not (yet) observed and at which timescale this second type of failure kinetics may become apparent. Therefore, a procedure to predict region II failure (slow crack growth) in creep tests, using region II failure data of fatigue tests (fatigue crack growth), is discussed in this section. Such a procedure implicitly assumes that the underlying mechanism for slow crack growth failure and fatigue crack growth failure is similar and can be described with the similar relations. In the next sections it is shown that it is important to take the influence of both the frequency (f) and the stress ratio (R) of the dynamic stress signal into account. The influence of frequency is studied using a relation proposed by Kim et al.[56] to describe the dynamic fatigue failure data in the next section. Subsequently, the influence of an increase of the stress ratio of the dynamic stress signal towards unity (=creep) on the fatigue crack growth is discussed.

Influence of frequency on fatigue crack growth

Region II failure for tensile bars under dynamic loads is generally attributed to fatigue crack growth. Most fatigue crack growth models are based upon the Paris law,[57] which relates the range of the stress intensity factor (ΔK_I) to the rate of crack propagation per cycle ($\frac{\mathrm{d}a}{\mathrm{d}N}$):

$$\frac{\mathrm{d}a}{\mathrm{d}N} = A\Delta K_I^m \,, \tag{14}$$

with A and m constants. Although these constants are sometimes assumed to be only material dependent, they are known to depend on the frequency[56,58–60] (f), stress ratio[61–63] (R), temperature[56,63,64] and molecular weight distribution.[65–67] The dynamic fatigue experiments presented in Figure 12 are conducted at a wide range of frequencies, which rules out the use of Equation (14) to completely describe the measured data set with the use of only one parameter set.[g] Therefore, a modification to Equation (14) as proposed by Kim et al.[56] is employed here. Their empirical relation takes the influence of frequency and temperature into account and is shortly summarised in Appendix C. The initial flaw size was used as a fit parameter, resulting in a value of 50 µm. This value is in agreement with the range of inherent defect sizes in uPVC pipes reported in other studies.[68,69]

The resulting calculated time-to-failure at different frequencies are shown in Figure 15 as solid lines. The good agreement between the experimental data (markers) and the

[g]The stress ratio R for the data in Figure 12 varies between 0.05 and 0.1. The experimental data of Kim et al.[61] suggests that the fatigue crack growth is only marginally influenced by the variation of R within this range. Therefore, this effect is neglected here.

model description supports the statement that the failure mechanism for failures after the knee is fatigue crack growth. The relation and parameters of Kim et al. accurately describe both the slope and the frequency dependence of the maximum stress versus time-to-failure. It is important to note that where failure in region I is insensitive for the frequency of the stress signal (as shown in Equation (13)), fatigue crack growth failures are influenced significantly by the frequency. A decrease in frequency results in an increase in the time-to-failure. The same data, plotted in Figure 15 (right) as a function of cycles-to-failure, shows a frequency dependent response for the failures in both region I and region II. The latter does not comply with the Paris law (Equation (14)), but is in agreement with the relation proposed by Kim et al.: the number of cycles-to-failure increases with an increase in frequency of the applied stress. These observations should be taken into account when estimating the slow crack growth rate from fatigue crack growth measurements, as discussed in the next section.

Influence of the stress ratio on fatigue crack growth

The stress ratio, R, of the dynamic signal influences the kinetics of Region II failures in uPVC[60, 70]. At the University of Leoben an approach has been developed that correlates the fatigue crack growth rate to the slow crack growth rate[6, 63]. They extrapolate fatigue crack growth kinetics for a range of stress ratios towards R=1 (creep). Here, a similar strategy is followed. Preliminary fatigue crack growth rate measurements were carried out on uPVC compact tension specimens. The crack growth rate was determined at four different stress ratios (from 0.1 up to 0.7). The results of the measurements are shown as markers in Figure 16, where the fatigue crack growth rate $\frac{\mathrm{d}a}{\mathrm{d}t}$ is plotted versus the maximum stress intensity factor K_{max}. A clear decrease in the crack growth rate is observed for an increase in R. The slope of the crack growth rate versus maximum stress intensity factor in a double logarithmic plot remains more or less constant for the range of stress ratios investigated. The solid lines represent the fatigue crack growth rates as predicted using Equation (C.1). The dashed lines represent the extrapolation of these results out of the range of K_{max} values in which Kim et al.[56] characterised their material. These extrapolated lines are in reasonable agreement with the experimental data for the range of maximum stress intensity factors lower than 5 MPa $\cdot$ m$^{0.5}$: the influence of R on the crack growth rate is similar and the lines coincide with the markers at K_{max}=3 MPa $\cdot$ m$^{0.5}$. Apparently, the molar mass of the material used by Kim et al. is comparable to that of the material used here.

The predictions of the time-to-failure at different (constant) values of R (again using an initial flaw size of 50 μm) are shown as solid lines in Figure 17. The predictions are in good agreement with the experimental data (shown as markers). As previously discussed, both the predictions of the yield lines and the measured ductile failure times

decrease with an increase in R. The failure time for crack growth failure (region II) is more sensitive to an increase in R and *increases*. For an increase in R from 0.1 to 0.5 the failure times increase about 1.2 decades (compared to a decrease of only about 0.3 decades for the yield failures).

The fatigue crack growth rate at a particular K_{max} (=3 MPa $\cdot$ m$^{0.5}$) is plotted against the stress ratio in Figure 18. The experimental data (shown as markers) and the model predictions using Equation (C.1) are in close agreement.[h] As Brown et al.[71] already noted, two regimes can be distinguished. At low stress ratios the crack growth rate is hardly influenced by a change in stress ratio, whereas at high stress ratio this influence on the crack growth ratio becomes much more pronounced. With the use of SAXS measurements they showed that at low R values the craze fibrils in polystyrene buckle during fatigue loading, due to compressive forces imposed by the material surrounding the crack tip on the fibrils. For ratios higher than about 0.6 the craze fibrils remain straight and the fibrils only contract in length and increase in diameter as the minimum stress level is approached. This difference in deformation behaviour of the fibrils can be the cause of a different failure mechanism, explaining the sharp decrease in crack growth rate as the stress ratio approaches unity.

The relation between R and $\frac{\mathrm{d}a}{\mathrm{d}t}$ is used to calculate the time-to-failure for uPVC subjected to a dynamic load with a stress ratio ranging from 0.1 up to 0.9. The resulting failure times are shown as solid lines in Figure 19. These lines lead to the important observation that with an increase in R the time-to-failure *decreases* slightly for region I failures, whereas , in region II, failure times *dramatically increase*. In region I, failure is dependent of the level of the applied stress. Failure thus occurs on shorter timescales for high R-values as the polymer is subject to a high stress for a longer part of the cycle. In region II, failure mainly depends on the amplitude of the stress. Specimens can sustain a cyclic load with a high R-value for longer periods of time as the amplitude of the stress signal decreases with an increase in R.

The predicted fatigue crack growth failure at R=0.9 becomes apparent after $5 \cdot 10^6$ s; significantly longer than the longest failure time measured by Niklas et al. at 20 °C for pipes subjected to a constant load (see Figure 8). This explains why the second region of failure kinetics was not observed in their experimental data. This observation complies with predictions of Truss[72] who estimated that region II failure occurs after at least $3 \cdot 10^9$ s for a well processed uPVC pipe at 20 °C.

The model cannot be used to obtain a realistic value for the slow crack growth rate as extrapolation towards R=1 leads to a crack growth rate of 0 m/s. The uPVC pipes used in the gas network are operated at a pressure of only 100 mbar resulting in a very low wall stress during their service life. The prediction at R=0.9 rules out slow

[h] In this case the frequency is kept constant and the use of Equation (14) with corresponding values for A and m would therefore result in identical results.

crack growth failure for these pipes within their service life. The water and sewer networks are, however, operated at higher and sometimes oscillating pressures. As a consequence, it is of interest for the water and sewer network operators to characterise and model region II failure kinetics.

More research is required to obtain a more reliable estimate of the slow crack growth kinetics of uPVC. The research should focus on characterising the influence of the stress ratio up to R-values close to unity. In a previous section it was shown that the frequency also influences the fatigue crack growth rate. As the frequency is undefined for a static signal, one should be careful in extrapolating fatigue crack growth rates measured at one frequency only. It is therefore imperative that the influence of frequency is taken into account when extrapolating towards R=1. Furthermore, it should be verified whether compressive forces at the crack tip for fatigue loads with a low stress ratio indeed results in a different failure mechanism than that occurring for fatigue failure at higher stress ratios. More knowledge on the failure mechanisms is required to improve the extrapolation procedure. Other approaches such as the one proposed by Hu et al.[60] may also be viable. They proposed a model where the (fatigue) crack growth rate is the product of a creep contribution, that depends only on the maximum stress intensity factor, and a fatigue contribution, that depends on the local strain rate. The slow crack growth rate follows from the creep contribution. Another issue that should be addressed is the temperature dependence of the crack growth failure mechanism. This temperature dependent response should be characterised, as the service temperature of uPVC pipes is generally lower than room temperature at which most laboratory experiments are conducted.

Conclusion

The influence of physical ageing on the resistance against plastic deformation is successfully implemented in a pressure-modified Eyring relation by making the pre-exponential factor a function of time. The influence of temperature and stress on the physical ageing kinetics was characterised using tensile yield stress measurements on specimens that were aged under different conditions. With the resulting parameters it is possible to predict long-term ductile failure for not only tensile bars, but also pipe segments subjected to a constant load. The endurance limit, observed for specimens that age significantly during the measurement, is also predicted accurately. The predictions for specimens subjected to a dynamic load are in reasonable agreement. Both the predictions and the measurements of the time to ductile failure are shown to be frequency independent. The engineering approach presented in this paper has the advantage that a less laborious characterisation procedure is required compared to the ones required for existing constitutive models that are also capable of producing

long-term failure predictions.

During the dynamic fatigue tests fatigue crack growth failure was observed as a second type of failure kinetics in the maximum stress versus time-to-failure plots. This fatigue crack growth failure appeared to be highly dependent on both the frequency and the stress ratio of the applied stress signal. Preliminary fatigue crack growth experiments suggest that slow crack growth failure does not occur within the service life of uPVC gas pipes. Additional research to the fatigue and slow crack growth behaviour of uPVC is required to confirm this preliminary estimate.

Acknowledgements: The financial support of *Cogas Infra B.V.*, *Enexis*, *Liander* and *Stedin* to carry out the presented research program is gratefully acknowledged by the authors.

Appendix A: Deduction of the time-to-failure under constant loads

The time-to-failure for a glassy polymer that is subjected to a constant load is calculated using the hypothesis that failure occurs after reaching a critical value of the equivalent plastic strain ($\bar{\gamma}_{cr}$), resulting in Equation (5). The rate of plastic strain accumulation including ageing kinetics is a function of time as given in Equation (4). Combining Equation (4) and (5) results in the following relation for the critical plastic strain, from which the time-to-failure for isothermal creep tests can be calculated:

$$\bar{\gamma}_{cr} = \frac{b_0}{t_0^{b_1}} \cdot \exp\left(\frac{-\Delta U - \mu p \nu^*}{RT}\right) \cdot \sinh\left(\frac{\bar{\tau}\nu^*}{RT}\right) \cdots \cdot \int_0^{t_f} \left(\frac{t'}{a_T(T) \cdot a_\sigma(T,\bar{\tau})} + t_a\right)^{b_1} \mathrm{d}t'. \quad \text{(A.1)}$$

An analytical solution can be found by substituting $x = \frac{t'}{a_T(T) \cdot a_\sigma(T,\bar{\tau})} + t_a$ and $\frac{\mathrm{d}x}{\mathrm{d}t'} = \frac{1}{a_T(T) \cdot a_\sigma(T,\bar{\tau})}$:

$$\begin{aligned} \frac{\bar{\gamma}_{cr} \cdot \exp\left(\frac{\Delta U + \mu p \nu^*}{RT}\right)}{b_0 \cdot t_0^{-b_1} \cdot \sinh\left(\frac{\bar{\tau}\nu^*}{RT}\right)} &= a_T(T) \cdot a_\sigma(T,\bar{\tau}) \cdot \int_{t_a}^{\frac{t_f}{a_T(T) \cdot a_\sigma(T,\bar{\tau})} + t_a} x^{b_1} \, \mathrm{d}x \\ &= \frac{a_T(T) \cdot a_\sigma(T,\bar{\tau})}{b_1 + 1} \cdot \left[\left(\frac{t_f}{a_T(T) \cdot a_\sigma(T,\bar{\tau})} + t_a\right)^{b_1+1} - t_a^{b_1+1}\right]. \end{aligned}$$

Rewriting this equation gives the analytical solution for the time-to-failure:

$$t_f(T,\bar{\tau}) = a_T(T)\cdot a_\sigma(T,\bar{\tau})\cdots \\ \cdot\left(\left[\frac{\bar{\gamma}_{cr}\cdot t_0^{b_1}\cdot\,(b_1+1)\,\cdot\exp\left(\frac{\Delta U}{RT}+\frac{\mu p\nu^*}{RT}\right)}{a_T(T)\cdot a_\sigma(T,\bar{\tau})\cdot b_0\cdot\,\sinh\left(\frac{\bar{\tau}\nu^*}{RT}\right)}+t_a^{b_1+1}\right]^{\frac{1}{b_1+1}}-t_a\right). \quad \text{(A.2)}$$

Appendix B: Analytical solution for a triangular waveform

A stress signal with a triangular waveform (see Figure 10), σ_{tria}, can be described with the continuous function:

$$\sigma_{tria}\,(t) = \sigma_m + \frac{2\sigma_{amp}}{\pi}\arcsin\Big(\sin(2\pi f t)\Big), \tag{B.1}$$

where σ_m is the mean stress, σ_{amp} the stress amplitude and f is the frequency. To find an analytical solution for the deformation and ageing kinetics for this wave form, a more appropriate, discontinuous function for the triangular waveform was used.

$$\sigma_{tria}\,(t) = A + Bt, \tag{B.2}$$

$$\text{with}\begin{cases} A = \sigma_m & \wedge \quad B = 4f\sigma_{amp} & \text{for} \quad 0 \le t < \frac{1}{4f} \\ A = \sigma_m + 2\sigma_{amp} & \wedge \quad B = -4f\sigma_{amp} & \text{for} \quad \frac{1}{4f} \le t < \frac{3}{4f} \\ A = \sigma_m - 4\sigma_{amp} & \wedge \quad B = 4f\sigma_{amp} & \text{for} \quad \frac{3}{4f} \le t < \frac{1}{f} \end{cases}.$$

Janssen et al.[55] already provided a solution for the acceleration factor of the deformation kinetics for a triangular wave (in tension) and with the approximation that $\sinh(x) \approx 0.5 \cdot \exp(x)$ for $x \gg 1$.

$$a_{\dot{\bar{\gamma}},tria} = \frac{3RT}{\left(\sqrt{3}+\mu\right)\cdot\nu^*\sigma_{amp}} \cdot \sinh\left(\frac{\left(\sqrt{3}+\mu\right)\cdot\nu^*\sigma_{amp}}{3RT}\right) \tag{B.3}$$

The acceleration factor for the aging kinetics can be calculated using Equation (12). Assuming isothermal conditions and combining the result with Equation (B.2) and (12) the relation is as follows:

$$a_{d,age} = a_\sigma(T, \frac{\sigma_m}{\sqrt{3}}) \cdot f \cdot \int_0^{\frac{1}{f}} \frac{\sqrt{3}RT}{(A+Bt)\cdot\nu_a} \cdot \sinh\left(\frac{(A+Bt)\cdot\nu_a}{\sqrt{3}RT}\right) \mathrm{d}t. \tag{B.4}$$

Using the substitutions σ_{tria}=$A + Bt$, $\mathrm{d}t$=$\frac{\mathrm{d}\sigma_{tria}}{B}$ and τ_a=$\frac{RT}{\nu_a}$, in Equation (B.4) results in:

$$a_{d,age} = \frac{\sqrt{3}f\tau_a a_\sigma(T, \frac{\sigma_m}{\sqrt{3}})}{B} \cdot \int_A^{A+\frac{B}{f}} \frac{\sinh\left(\frac{\sigma_{tria}}{\sqrt{3}\tau_a}\right)}{\sigma_{tria}} \mathrm{d}\sigma_{tria}. \tag{B.5}$$

For the analytical solution the following standard integral will be used:

$$\int \frac{\sinh(ax)}{x}\mathrm{d}x = \sum_{n=0}^{\infty} \frac{(ax)^{2n+1}}{(2n+1)(2n+1)!} = F(x). \tag{B.6}$$

Applying this relation and solving it for each of the three sections of the wave results in:

$$a_{d,age} = \frac{\sqrt{3} f \tau_a a_\sigma(T, \frac{\sigma_m}{\sqrt{3}})}{4 f \sigma_{amp}} \cdot \left(\underbrace{F(\sigma_m + \sigma_{amp}) - F(\sigma_m)}_{0 \leq t < \frac{1}{4f}} \cdots \right.$$

$$\left. - \underbrace{F(\sigma_m - \sigma_{amp}) - F(\sigma_m + \sigma_{amp})}_{\frac{1}{4f} \leq t < \frac{3}{4f}} + \underbrace{F(\sigma_m) - F(\sigma_m - \sigma_{amp})}_{\frac{3}{4f} \leq t < \frac{1}{f}} \right) . \quad \text{(B.7)}$$

This can be reduced to the final solution:

$$a_{d,age} = \frac{\sqrt{3} R T a_\sigma(T, \frac{\sigma_m}{\sqrt{3}})}{2 \nu_a \sigma_{amp}} \cdots$$

$$\cdot \left(\sum_{n=0}^{\infty} \frac{\left(\frac{\nu_a \sigma_{max}}{\sqrt{3} R T} \right)^{2n+1}}{(2n+1)(2n+1)!} - \sum_{n=0}^{\infty} \frac{\left(\frac{\nu_a \sigma_b}{\sqrt{3} R T} \right)^{2n+1}}{(2n+1)(2n+1)!} \right) . \quad \text{(B.8)}$$

Appendix C: Summary of fatigue crack growth model

Kim et al.[56] proposed a modified version of the Paris law to take the influence of frequency and temperature on the fatigue crack growth kinetics of uPVC into account:

$$\frac{\mathrm{d}a}{\mathrm{d}N} = \left(\frac{f}{f_{ref}}\right)^{-n} \cdot \left[B \cdot \exp\left(-\frac{\Delta H_{th} - \gamma \cdot \log \Delta K_I}{RT}\right)\right]_{ref}. \tag{C.1}$$

The subscript "$_{ref}$" denotes an arbitrarily chosen reference point, ΔH_{th} the apparent activation energy and both n and γ (not to be confused with a strain) are constants. For a reference frequency of 1 Hz, the experimental data of Kim et al.[56] was best described with the values ΔH_{th}=43.6 kJ $\cdot$ mol^{-1}, B=3.75 $\cdot$ 10^{12}, γ=16.5 kJ $\cdot$ mol^{-1} and n=0.295. These parameters were also used to describe the dynamic fatigue data as obtained in this study, although it is unknown whether the material used in the study of Kim et al. is comparable with the material used throughout the present study.

The stress intensity factor range is defined as:

$$\Delta K_I = K_{I,max} - K_{I,min} = (\sigma_{max} - \sigma_{min}) \cdot Y\sqrt{a}, \tag{C.2}$$

where Y is a geometrical factor. The geometrical factor for the tensile bars as used in the current study can be calculated with the empirical solution for a Single End Notched Beam (SENB) specimen subjected to tensile loads:

$$Y = \frac{\sqrt{2w \cdot \tan\left(\frac{\pi a}{2w}\right)}}{\sqrt{a} \cdot \cos\left(\frac{\pi a}{2w}\right)} \cdot \left(0.752 + 2.02 \cdot \frac{a}{w} + 0.37 \cdot \left[1 - \sin\left(\frac{\pi a}{2w}\right)\right]^3\right), \tag{C.3}$$

where w is the width of the specimen, which is chosen to be equal to the wall thickness of the original pipe (≈4.1 mm) as most cracks in the tensile bars grow in the radial direction of the original pipe geometry. The cycles to failure follow from solving differential Equation (C.1) for the initial crack size up to the critical crack size. This critical crack size taken as the crack size at which K_{max} is equal to the critical stress intensity factor ($K_{Ic} \approx 4$ MPa $\cdot \sqrt{\mathrm{m}}$ for PVC[73]). The initial crack size (a_{ini}) was used as a fit parameter. The experimental data is accurately described with a value of a_{ini}=50 μm.

Acknowledgements: The financial support of *Cogas Infra B.V.*, *Enexis*, *Liander* and *Stedin* to carry out the presented research program is gratefully acknowledged by the authors.

Received: ; Revised: ; Published online: ;
DOI:

Keywords: ageing; failure; fatigue analysis; poly(vinyl chloride) (PVC); yielding

References

[1] H. Montiel, J.A. Vílchez, J. Arnaldos, J. Casal, *J. Hazard. Mater.* , **1996**, *51*, 77.
[2] N. Piccinini, R. Tommasini, E. Pons, *Process Saf. Environ.* , **2009**, *87*, 73.
[3] R.W. Lang, A. Stern, G. Doerner, *Angew. Makromol. Chem.* , **1997**, *247*, 131.
[4] G. Castiglioni, D. Verzanini, A. Pavan, *Plastic Pipes XII*, Baveno.
[5] N. Brown, *Polym. Eng. Sci.* , **2007**, *47*, 477.
[6] G. Pinter, R.W. Lang, M. Haager, *Monatsh. Chem.* , **2007**, *138*, 347.
[7] U.W. Gedde, J. Viebke, H. Leijström, M. Ifwarson, *Polym. Eng. Sci.* , **1994**, *34*, 1773.
[8] U. Andersson, *Plastic Pipe XI*, Munchen.
[9] H.A. Visser, T.C. Bor, M. Wolters, T.A.P. Engels, L.E. Govaert, *Macromol. Mater. Eng.* , **2010**, *295*.
[10] A. Gray, J.N. Mallinson, J.B. Price, *Plast. Rub. Proc. Appl.* , **1981**, *1*, 51.
[11] J.P. Lu, P. Davis, L.S. Burn, *Polym. Eng. Sci.* , **2003**, *43*, 444.
[12] H. Vogt, H.-F. Enderle, U. Schulte, J. Hessel, *Plastic Pipes XIV*, Budapest.
[13] K.S. Minsker, G.E. Zaikov, *J. Vinyl Addit. Techn.* , **2001**, *7*, 222.
[14] M. Schiller, W. Fischer, *Plastic Pipes XII*, Baveno.
[15] P. Benjamin, *Plast. Rubber Mater. Appl.* , **1980**, *5*, 151.
[16] B. Terselius, J.-F Jansson, *Plast. Rub. Proc. Appl.* , **1984**, *4*, 285.
[17] H. Niklas, H.H. Kausch von Schmeling, *Kunststoffe* , **1963**, *53*, 886.
[18] J.M. Hutchinson, *Prog. Polym. Sci.* , **1995**, *20*, 703.
[19] J.H. Golden, B.L. Hammant, E.A. Hazell, *J. Appl. Polym. Sci.* , **1967**, *11*, 1571.
[20] T.E. Brady, G.S.Y. Yeh, *J. Appl. Phys.* , **1971**, *42*, 4622.
[21] A. Cross, R.N. Haward, N.J. Mills, *Polymer* , **1979**, *20*, 288.
[22] H.G.H. van Melick, L.E. Govaert, H.E.H. Meijer, *Polymer* , **2003**, *44*, 3579.
[23] H.X. Li, C.P. Buckley, *Int. J. Solids Struct.* , **2009**, *46*, 1607.
[24] E.J. Kramer, *Adv. Pol. Sci.* , **1983**, *52/53*, 1.
[25] P.J.F. van den Heuvel, *Plastic Pipes V*, York.
[26] E.T.J. Klompen, T.A.P. Engels, L.C.A. van Breemen, P.J.G. Schreurs, L.E. Govaert, H.E.H. Meijer, *Macromolecules* , **2005**, *38*, 7009.
[27] J. Worp, *Het Gas* , **1957**, *78*, 2.
[28] D.H. Ender, R.D. Andrews, *J. Appl. Phys.* , **1965**, *36*, 3057.
[29] D.J. Matz, W.G. Guldemond, S.I. Cooper, *J. Polym. Sci. Pol. Phys.* , **1972**, *10*, 1917.
[30] K.V. Gotham, S. Turner, *Polym. Eng. Sci.* , **1973**, *13*, 113.
[31] E.T.J. Klompen, T.A.P. Engels, L.E. Govaert, H.E.H. Meijer, *Macromolecules* , **2005**, *38*, 6997.
[32] I.M. Ward, *J. Mater. Sci.* , **1971**, *6*, 1397.

[33] D.J. Matz, W.G. Guldemond, S.I. Cooper, *Polym. Eng. Sci.* , **1973**, *13*, 300.
[34] C. Bauwens-Crowet, J.C. Bauwens, *Polymer* , **1982**, *23*, 1599.
[35] C. Ho Huu, T. Vu-Khanh, *Theor. Appl. Fract. Mec.* , **2003**, *40*, 75.
[36] P.I. Vincent, *Polymer* , **1960**, *1*, 7.
[37] E.J. Kramer, *J. Appl. Phys.* , **1970**, *41*, 7.
[38] F.A. Myers, F.C. Cama, S.S. Sternstein, *Ann. New York Acad. Sci.* , **1976**, *279*, 94.
[39] E.R. Harrell, Jr., R.P. Chartoff, *J. Macromol. Sci. -Phys.* , **1977**, *B14*, 277.
[40] Y. Nanzai, A. Miwa , **1999**, *42*, 479.
[41] E.R. Harrell, Jr., R.P. Chartoff, *Polym. Eng. Sci.* , **1974**, *14*, 362.
[42] C. Tsitsilianis, M. Tsapatsis, Ch. Economou, *Polymer* , **1989**, *60*, 1861.
[43] T.A. Tervoort, E.T.J. Klompen, L.E. Govaert, *J. Rheol.* , **1996**, *40*, 779.
[44] P. Benjamin, *J. Vinyl Techn.* , **1980**, *2*, 254.
[45] G.C. Portingell, *Particulate nature of PVC; Formation structure and processing*, G. Butters, ed., Applied Science Publishers ltd., London, **1982**, 135–234.
[46] J. Parey, G. Menges, *J. Vinyl Techn.* , **1981**, *3*, 152.
[47] R.J.M. Hermkens, M. Wolters, J. Weller, H.A. Visser, *Plastic Pipes XIV*, Budapest.
[48] B. Terselius, J.-F Jansson, J. Bystedt, *Plast. Rub. Proc. Appl.* , **1985**, *5*, 1.
[49] B. Terselius, J.-F Jansson, *Plast. Rub. Proc. Appl.* , **1984**, *4*, 291.
[50] J.A. Covas, M. Gilbert, D.E. Marshall, *Plast. Rub. Proc. Appl.* , **1988**, *9*, 107.
[51] R.W. Truss, *Pure Appl. Chem.* , **1985**, *57*, 993.
[52] J.W. Summers, E.B. Rabinovitch, J.G. Quisenberry, *J. Vinyl Techn.* , **1982**, *4*, 67.
[53] G.P. Marshall, S. Brogden, M.A. Shepherd, *Plast. Rub. Compos. Pro.* , **1998**, *27*, 483.
[54] R.P.M. Janssen, D. de Kanter, L.E. Govaert, H.E.H. Meijer, *Macromolecules* , **2008**, *41*, 2520.
[55] R.P.M. Janssen, L.E. Govaert, H.E.H. Meijer, *Macromolecules* , **2008**, *41*, 2531.
[56] H.S. Kim, X.M. Wang, *J. Mater. Sci.* , **1994**, *29*, 3209.
[57] P. Paris, F. Erdogan, *J. Basic Eng.* , **1963**, *85*, 528.
[58] R.W. Hertzberg, J.A. Manson, M. Skibo, *Polym. Eng. Sci.* , **1975**, *15*, 252.
[59] J.C. Radon, *J. Macromol. Sci. -Phys.* , **1977**, *B14*, 511.
[60] Y. Hu, J. Summers, A. Hiltner, E. Baer, *J. Mater. Sci.* , **2003**, *38*, 633.
[61] H.S. Kim, R.W. Truss, Y.W. Mai, B. Cotterell, *Polymer* , **1988**, *28*, 268.
[62] H.S. Kim, Y.W. Mai, B. Cotterell, *J. Mater. Sci.* , **1993**, *28*, 3367.
[63] W. Balika, R.W. Lang, *Macromol. Symp.* , **2002**, *181*, 341.
[64] H.-S. Kim, Y.-W. Mai, *J. Mater. Sci.* , **1993**, *28*, 5479.
[65] M. Skibo, J.A. Manson, R.W. Hertzberg, E.A. Collins, *J. Macromol. Sci. -Phys.* , **1977**, *B14*, 525.

[66] C.M. Rimnac, J.A. Manson, R.W. Hertzberg, S.M. Webler, M.B. Skibo, *J. Macromol. Sci. -Phys.* , **1981**, *B19*, 351.

[67] T.E. Bernal-Lara, Y. Hu, J. Summers, A. Hiltner, E. Baer, *J. Vinyl Addit. Techn.* , **2004**, *10*, 5.

[68] H.J.M. Rijpkema, M. Wolters, *Plastics Pipes VIII*, Koningshof.

[69] S. Burn, P. Davis, T. Schiller, B. Tiganis, G. Tjandraatmadja, M. Cardy, S. Gould, P. Sadler, A.J. Whittle, Long-term performance prediction for pvc pipes, Technical report, Awwa research foundation, **2006**.

[70] J.F. Mandell, J.-P.F. Chevaillier, *Polym. Eng. Sci.* , **1985**, *25*, 170.

[71] H.R. Brown, E.J. Kramer, R.A. Bubeck, *J. Mater. Sci.* , **1988**, *23*, 248.

[72] R.W. Truss, *Plast. Rub. Proc. Appl.* , **1987**, *7*, 51.

[73] L.R. Holloway, A.J. Naaktgeboren, *Pipes Pipelines Int.* , **1990**, *35*, 32+34.

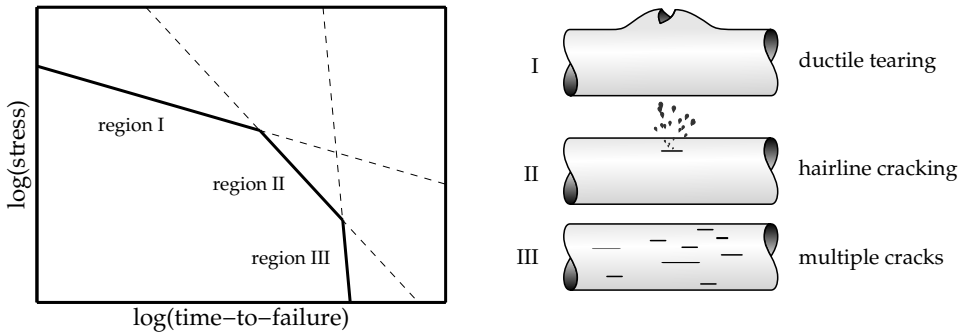

Figure 1. Left: schematic representation of typical results from burst pressure tests. Right: the three failure modes that can occur during burst pressure tests.

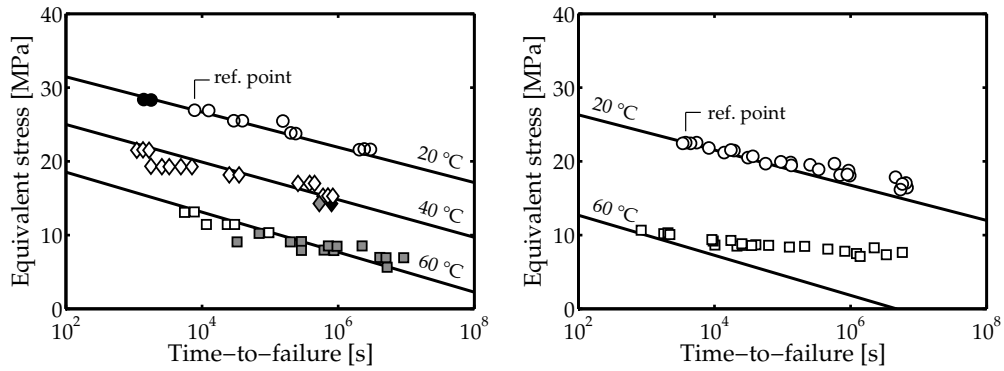

Figure 2. Time-to-failure data for PVC pipes subjected to an internal pressure. The three failure types (ductile tearing, hairline cracking and brittle fracture) are shown with white, grey and black filled markers, respectively. The solid lines represent predictions of the approach presented in a previous paper.[9] Left: Predictions for data from Niklas et al.[17] Right: Predictions for ductile failure data of Benjamin. [15]

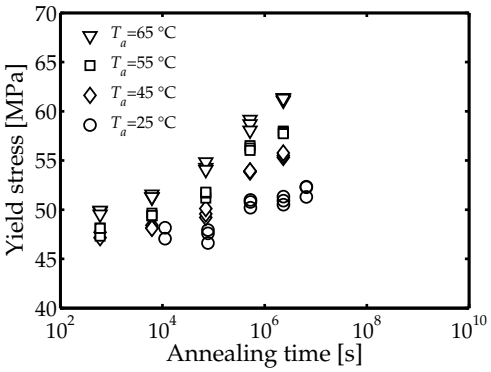

Figure 3. Tensile yield stress data of uPVC measured at a strain rate of 10^{-3} s^{-1} and a temperature of 25 °C, after annealing at different temperatures. The yield stress is plotted against the annealing time.

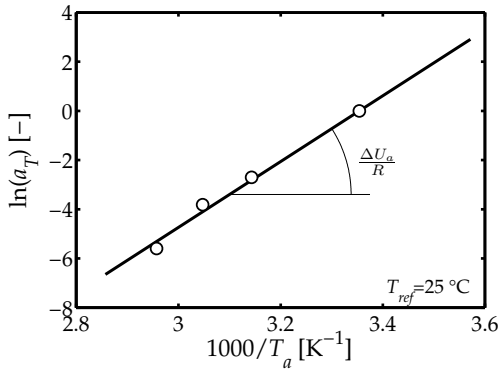

Figure 4. The natural logarithm of the shift factor versus the annealing temperature. The factor a_T is defined in this figure as the factor required to shift the yield data for the different annealing times on top of the yield data for the specimens annealed at 25 °C. The activation energy (ΔU_a) in Equation (6) can be calculated from slope the of the solid line.

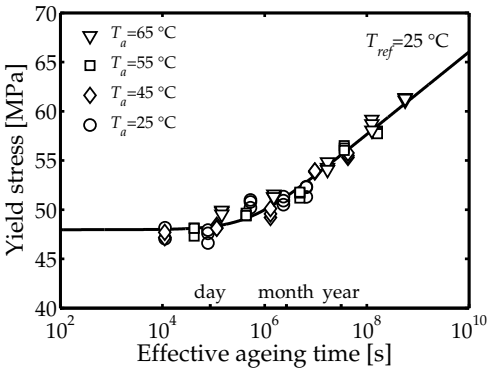

Figure 5. Reproduction of the yield stress data shown in Figure 3, but plotted against the effective ageing time at a reference temperature of 25 °C, using an activation energy of 115 kJ · mol^{-1} as calculated from the slope in Figure 4.

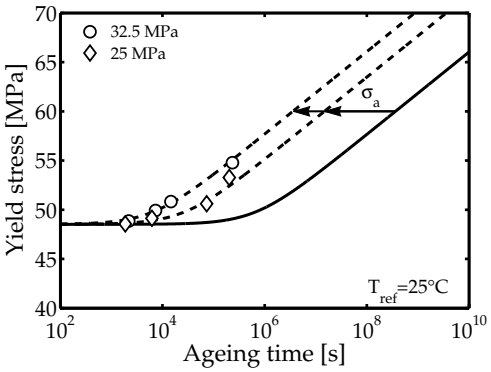

Figure 6. Tensile yield stress of uPVC at a strain rate of 10^{-3} s^{-1} and a temperature of 25 °C, after ageing the specimens at a tensile stress of 25 MPa or 32.5 MPa for a range of ageing times. The solid line represents the mastercurve for uPVC at 25 °C. The dashed lines show the shifted mastercurve to the ageing condition of the respective specimens. For the shift as given by Equation (7) an activation volume (ν_a) of $9.65 \cdot 10^{-4}$ $m^3 \cdot mol^{-1}$ has been used.

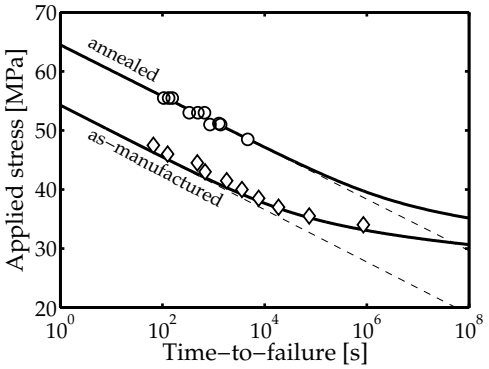

Figure 7. The time-to-failure for uPVC under a constant uniaxial load for annealed (at 20 °C) and as-manufactured (at 24 °C) specimens. The predictions employing Equation (8) that includes the influence of physical ageing are shown as solid lines and the predictions excluding ageing are shown as dashed lines.

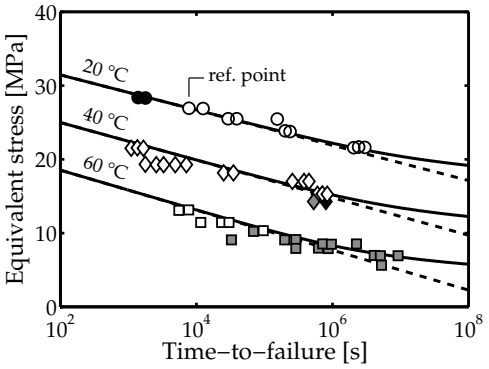

Figure 8. Time-to-failure for uPVC pipes subjected to an internal pressure as measured at three temperatures (reproduced from Niklas et al.[17]). The white, grey and black filled markers represent the failure modes ductile rupture, hairline cracking and brittle fracture respectively. Predictions with the approach including the influence of physical ageing on the deformation kinetics are shown in solid lines and predictions excluding ageing effects in dashed lines.

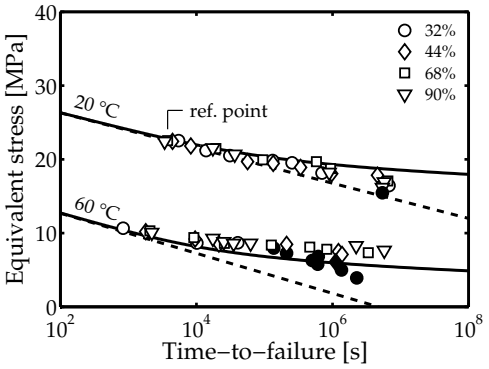

Figure 9. Time-to-failure for uPVC pipes subjected to an internal pressure and measured at two temperatures (reproduced from Benjamin[15]). The white filled markers represent ductile failures and the black filled markers represent brittle failures. Predictions with the approach including the influence of physical ageing on the deformation kinetics are shown in solid lines and predictions excluding ageing effects in dashed lines.

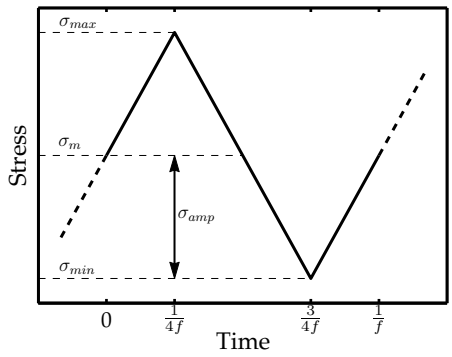

Figure 10. Schematic representation of a triangular waveform of the stress as a function of time, including the definitions for the maximum (σ_{max}), mean (σ_m) and minimum stress (σ_{min}), the stress amplitude (σ_{amp}) and the frequency (f).

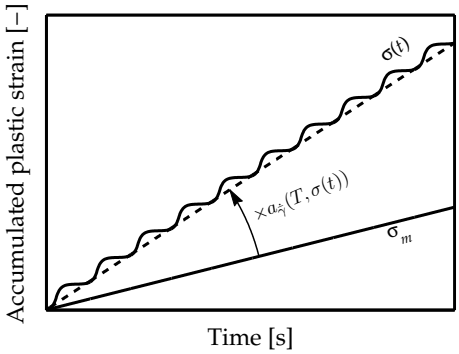

Figure 11. The accumulation of the plastic strain for a triangular waveform, $\sigma(t)$, and a constant load equal to the mean stress of the triangular waveform (σ_m), shown in solid black lines. The accumulation of the plastic strain for a triangular stress signal as calculated using the acceleration factor ($a_{d,\dot{\bar{\gamma}}}$) is shown as a dashed line.

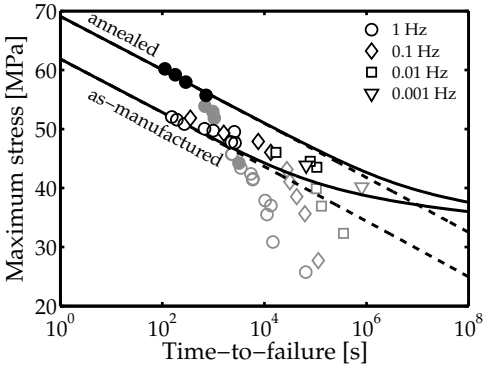

Figure 12. Time-to-failure for uPVC tensile specimens subjected to a triangular stress load at various frequencies. The minimum stress level is kept at a constant value of 2.5 MPa. The as-manufactured specimens (open markers) did not receive any additional heat treatment, whereas the annealed specimens (black filled markers) were annealed for $2.2 \cdot 10^6$ s at 60 °C. The specimens that failed as a result of fatigue crack growth are shown as grey markers.

.

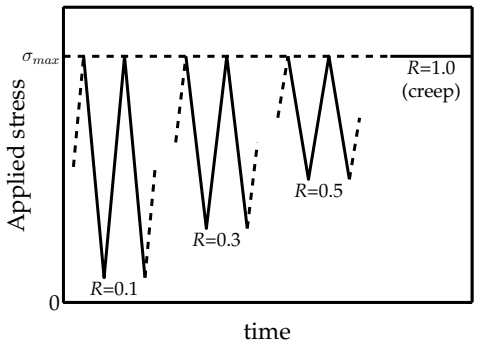

Figure 13. Schematic representation of the applied stress signal for three values for R, compared with a creep signal.

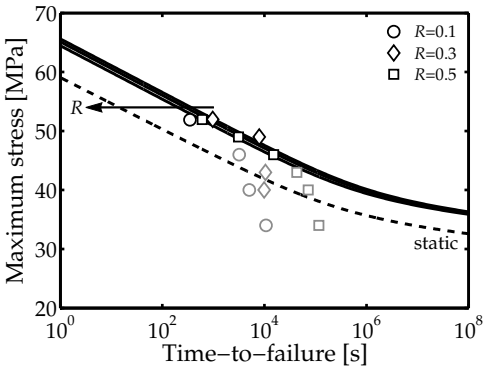

Figure 14. Time-to-failure for uPVC tensile specimens subjected to a triangular stress load at a frequency of 1 Hz and for three R values: 0.1, 0.3, 0.5 at 23 °C. The solid lines represent model predictions for the three values of R. The dashed line is a prediction for the failure time of these specimens, subjected to a static load (creep, R=1).

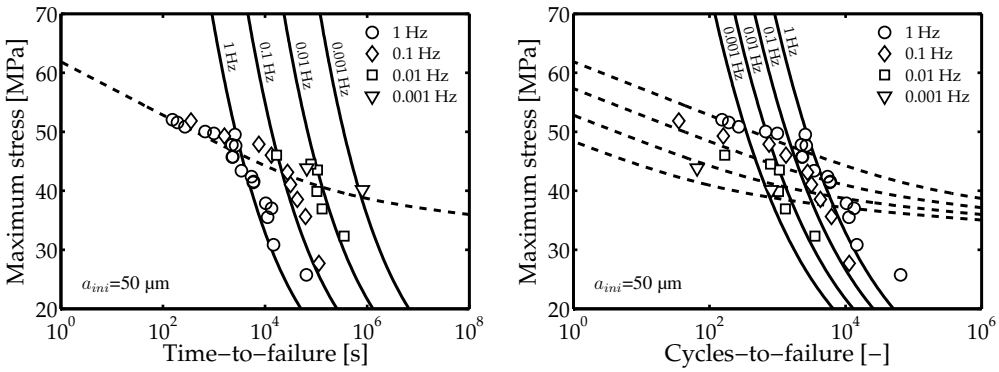

Figure 15. Reproduction of the data for the as-manufactured specimens from Figure 12 including failure predictions for Region II failure (solid lines) using the fatigue crack growth model of Kim et al.[56] and an initial defect size of 50 µm. The yield failure predictions are shown as dashed lines. Left: the maximum stress is plotted against the time-to-failure. Right: the maximum stress is plotted against the cycles-to-failure (N_f).

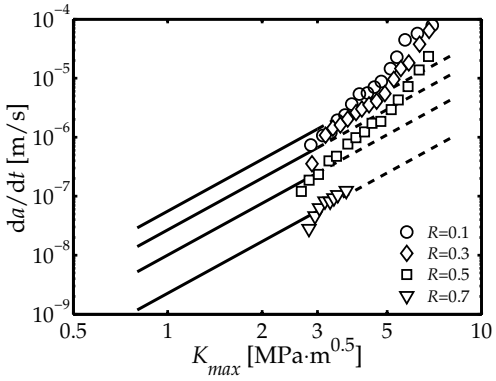

Figure 16. The crack growth rate of uPVC compact tension specimens versus the maximum stress intensity factor (K_{max}) on a double logarithmic scale for four different values for R and at a frequency of 1 Hz. The lines are calculated using Equation (C.1).

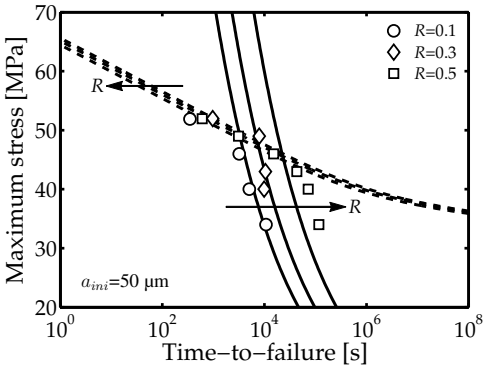

Figure 17. Reproduction of Figure 14 including failure predictions for Region II failure (solid lines) using the fatigue crack growth model of Kim et al.[56] and an initial defect size of 50 µm. The yield failure predictions are shown as dashed lines.

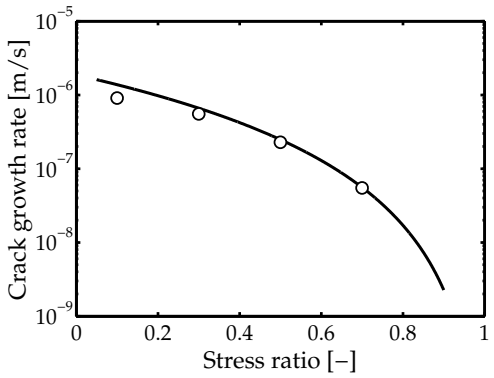

Figure 18. Extrapolation towards R=1; the crack growth rate at K_{max}=3 MPa $\cdot$ m$^{0.5}$ versus the stress ratio. The solid line represents the prediction of the model of Kim et al.[56] and the markers represent the measured crack growth rates at a frequency of 1 Hz.

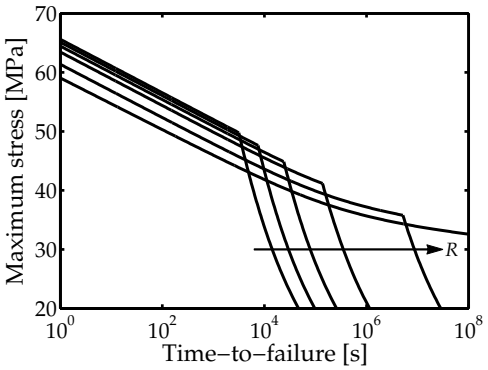

Figure 19. The predicted time-to-failure for dynamic stress signals with stress ratios of 0.1, 0.3, 0.5, 0.7 and 0.9 using the presented engineering approach and the model of Kim et al.[56]

Table 1. Definition of the equivalent plastic strain rate $\dot{\bar{\gamma}}$, the equivalent stress $\bar{\tau}$ and the hydrostatic pressure p as used in Equation (1) as a function of the strain tensor and stress tensor.

Definitions
$\dot{\bar{\gamma}} = \sqrt{2 \cdot (\dot{\epsilon}_{11}^2 + \dot{\epsilon}_{22}^2 + \dot{\epsilon}_{33}^2 + 2\dot{\epsilon}_{12}^2 + 2\dot{\epsilon}_{23}^2 + 2\dot{\epsilon}_{31}^2)}$
$\bar{\tau} = \sqrt{\frac{1}{6} \cdot \left[(\sigma_{11} - \sigma_{22})^2 + (\sigma_{22} - \sigma_{33})^2 + (\sigma_{33} - \sigma_{11})^2\right] + \sigma_{12}^2 + \sigma_{23}^2 + \sigma_{13}^2}$
$p = -\frac{1}{3} \cdot (\sigma_{11} + \sigma_{22} + \sigma_{33})$

Table 2. The values for the parameters for uPVC used in this work.

μ= 0.14	[-]†	b_0= $1.13 \cdot 10^{44}$	[s^{-1}]
ν^*= $2.06 \cdot 10^{-3}$	[$m^3 \cdot mol^{-1}$]†	b_1= -0.95	[-]
ΔU= $2.97 \cdot 10^5$	[$J \cdot mol^{-1}$]†	ΔU_a= $1.15 \cdot 10^5$	[$J \cdot mol^{-1}$]
$\bar{\gamma}_{cr}$= 0.015	[-]†	ν_a= $9.65 \cdot 10^{-4}$	[$m^3 \cdot mol^{-1}$]

† Value determined in Visser et al.[9]

Table 3. Relations for the equivalent stress and hydrostatic pressure as defined in Table 1 for uniaxial tension and a pipe with outer diameter D and wall thickness t subjected to an internal pressure (p_i).

	Uniaxial tension	Internal pressure
$\bar{\tau}$	$\frac{\sigma}{\sqrt{3}}$	$\frac{(D-2t)\cdot p_i}{4t}$
p	$-\frac{\sigma}{3}$	$-\frac{(D-2t)\cdot p_i}{4t}$

DOI:
Article type: Full paper

Table of contents entry.
By incorporating the influence of physical ageing in a previously presented model for the prediction of ductile failure in glassy polymers, it is possible to predict the so-called endurance limit that is observed for several glassy polymers. The model proves to be applicable to (ductile) fatigue failure as well. Additionally, the differences between the frequency and stress ratio dependence of ductile and fatigue crack growth failure are presented.

Table of contents and summary figure

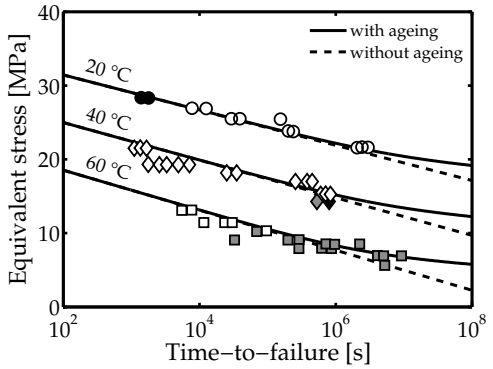

Authors
H.A. Visser, T.C. Bor, M. Wolters, J.G.F. Wismans, L.E. Govaert*

Title
Lifetime assessment of load-bearing polymer glasses; The influence of physical ageing